

promoting access to White Rose research papers



Universities of Leeds, Sheffield and York
<http://eprints.whiterose.ac.uk/>

This is an author produced version of a paper published in **Physica D-Nonlinear Phenomena**.

White Rose Research Online URL for this paper:
<http://eprints.whiterose.ac.uk/8738/>

Published paper

Clayton, R.H (2009) *Influence of cardiac tissue anisotropy on re-entrant activation in computational models of ventricular fibrillation*. Physica D-Nonlinear Phenomena, 238 (11-12). pp. 951-961.

Influence of cardiac tissue anisotropy on re-entrant activation in computational models of ventricular fibrillation

Richard H. Clayton

Department of Computer Science, University of Sheffield, United Kingdom

Corresponding author:

Dr Richard Clayton.

Address: Department of Computer Science,
University of Sheffield,
Regent Court,
211 Portobello Street,
Sheffield S1 4DP

Telephone: +44 (0)114 222 1845

Fax: +44 (0)114 222 1810

Email r.h.clayton@sheffield.ac.uk

Abstract

The aim of this study was to establish the role played by anisotropic diffusion in (i) the number of filaments and epicardial phase singularities that sustain ventricular fibrillation in the heart, (ii) the lifetimes of filaments and phase singularities, and (iii) the creation and annihilation dynamics of filaments and phase singularities. A simplified monodomain model of cardiac tissue was used, with membrane excitation described by a simplified 3-variable model. The model was configured so that a single re-entrant wave was unstable, and fragmented into multiple re-entrant waves. Re-entry was then initiated in tissue slabs with varying anisotropy ratio. The main findings of this computational study are: (i) anisotropy ratio influenced the number of filaments sustaining simulated ventricular fibrillation, with more filaments present in simulations with smaller values of transverse diffusion coefficient, (ii) each re-entrant filament was associated with around 0.9 phase singularities on the surface of the slab geometry, (iii) phase singularities were longer lived than filaments, and (iv) the creation and annihilation of filaments and phase singularities were linear functions of the number of filaments and phase singularities, and these relationships were independent of the anisotropy ratio. This study underscores the important role played by tissue anisotropy in cardiac ventricular fibrillation.

PACS numbers: 87.19.Hh, 87.85.Tu, 87.85.Xd, 87.18.Hf

Keywords: Cardiac arrhythmia, re-entry, ventricular fibrillation, excitable medium, spatiotemporal complexity

Introduction

The heart is an electromechanical pump, and propagating action potentials originating in the heart's pacemaker act to both trigger and synchronise the contraction associated with each heart beat. Disturbances of electrical activation in the heart are manifest as cardiac arrhythmias, and the most catastrophic of these is ventricular fibrillation (VF). VF is a state of electrical anarchy in which the regularity of normal rhythm is overthrown by rapid and self sustaining electrical activity. VF is deadly unless a normal rhythm can be restored by defibrillation, and is implicated as the lethal event in cases of sudden cardiac death.

The electrical mechanisms that initiate and sustain VF have been investigated in experimental studies using contact electrodes [1, 2] and voltage sensitive fluorescent dyes [3-5]. These observations have been limited to observations of activation in a region of tissue close to the surface, and are recognised as a surface projection of complex activation patterns within the thick walled ventricle [6, 7]. Although it remains difficult to extract information about 3D wavefronts during VF in experimental preparations, recent studies report progress in understanding how optical signals are produced [8], and the use of transillumination and tomography to obtain 3D information . Although some progress has been made with mapping activity within the thick walled ventricle [9, 10]. Modelling and simulation remain a valuable tool for explaining and interpreting experimental activation patterns, and for evaluating new experimental approaches.

Cardiac tissue behaves as a spatially extended excitable medium, and supports rotating re-entrant waves (also referred to as vortices or rotors) that have been observed in other excitable media including slime moulds [11] and the autocatalytic Belousov Zhabotinski reaction [11]. In 2D a re-entrant wave is a

spiral rotating around a point of phase singularity (PS), and in 3D a scroll shaped wavefront rotates around a line of phase singularity called a filament [12]. Experimental studies in cardiac tissue indicate that VF is sustained by multiple re-entrant waves, each rotating around a filament. These filaments interact with each other and with the tissue surface; producing an ever-changing 3D activation pattern within the tissue and a complex activation pattern on the 2D tissue surface. A surface PS is observed where a filament touches the tissue surface, and interacting mobile filaments within the tissue provide an explanation for the rapidly moving and short lived re-entry that is observed on the heart surface during VF [13, 14]. Figure 1 illustrates example surface patterns and underlying 3D activation during VF in a computational model.

Since filaments are difficult to observe directly, the number of filaments present during VF in the heart remains speculative. Based on experimental observation of PS in animal hearts, the number of rotors sustaining VF was estimated to be between 1 and 2 for the rabbit heart, around 5 for a sheep heart, and around 15 for the human heart [5]. A recent model of VF in the human heart predicts between 8 and 11 filaments manifest as between 5 and 7 epicardial PS, with a ratio of surface PS to filaments of between 0.71 and 0.77 [15]. Remarkably, this model prediction is in agreement with the number of epicardial PS observed in epicardial mapping experiments, where the median number of PS during VF was 7 ± 4 [2].

Cardiac myocytes are rod-shaped cells that are aligned in fibres and sheets within the tissue, and fibre orientation varies by about 120° across the ventricular wall [16]. Action potential propagation in cardiac tissue is strongly influenced by tissue anisotropy, and the conduction velocity longitudinal to fibres is approximately twice as large as the conduction velocity transverse to fibres. The ratio of longitudinal to transverse conduction velocity as well as gradients in fibre

orientation are known to influence both the stability of a re-entrant wave and the interactions of multiple re-entrant waves [17]. In addition a recent study of VF in the human heart, which used detailed models of both anatomy and excitability, found that the ratio of surface PS to filaments depended on tissue anisotropy [15]. The focus of the present study was therefore to examine this relationship in detail, using a computational model to quantify the effects of anisotropy ratio on (i) numbers of filaments and surface PS, and their ratio, (ii) the lifetimes of filaments and PSs, and (iii) the creation and annihilation dynamics of filaments and PS.

Methods

This study used a simplified model of excitation, combined with a slab geometry that represented a part of the left ventricular free wall.

Computational model

The electrophysiology of cardiac tissue was simulated using the monodomain equation, with membrane voltage V_m obtained from

$$\frac{\partial V_m}{\partial t} = \nabla \cdot (\mathbf{D} \nabla V_m) - \frac{I_{ion}}{C_m} \quad , \quad (1)$$

where C_m is specific membrane capacitance, \mathbf{D} a diffusion coefficient or tensor, and I_{ion} current flow through the cell membrane per unit area.

Many cell models have been developed that reproduce the action potential of cardiac cells from different species, and from different parts of the heart. Biophysically detailed cell models are computationally demanding to solve, and so

this study used a 3-variable simplified ionic model (3V-SIM) to describe I_{ion} . This model is described in detail elsewhere [17-21]. Briefly, total current density in the cell membrane is modelled as the sum of three components, J_{fi} , J_{si} and J_{so} . J_{fi} and J_{si} are fast and slow inward currents corresponding broadly to the inward currents carried by Na^+ and Ca^{2+} ions in real cardiac cells. J_{so} is a slow outward current broadly corresponding to outward currents carried by K^+ ions in real cardiac cells. J_{so} , J_{fi} and J_{si} are governed by two internal variables v , and w , and V_m is rescaled to be a dimensionless activation parameter, u , that varies between 0 and 1. The 0 to 1 range of u maps onto a voltage range of -85 to +15 mV.

We used the parameter set given in Table 1, which resulted in steep rate dependence of action potential duration (APD restitution). Figure 2(a) shows the APD and conduction velocity (CV) restitution for this variant of the 3V-SIM model. The APD restitution slope was close to 1, and when re-entry was initiated in a 2D tissue sheet it broke up into multiple wavelets as shown in Figure 2(b). Instability resulting from steep APD restitution is recognised as one mechanism that can result in the multiple re-entrant waves that can sustain VF [18, 22]. The periods of the three rotations prior to breakup (the second, third and fourth action potentials in Figure 2(c)) were 183, 100, and 77 ms.

Anisotropic diffusion

The components of the diffusion tensor for anisotropic diffusion in the monodomain model described above are given by:

$$D = \frac{G}{S_v C_m} , \quad (2)$$

where S_v is the surface volume ratio of cells, C_m the specific capacitance, and G is the corresponding component of the bulk conductivity tensor. Typical values of S_v for the mammalian heart are around 1000 cm^{-1} , and values in the range 200 to 3000 cm^{-1} have been used in computational studies [23]. The bulk conductance of cardiac tissue is difficult to measure precisely, because the intracellular and extracellular components have different anisotropy. Measurements of longitudinal and transverse intracellular conductivity range from 1.74 to 3.44 mS cm^{-1} and 0.193 to 0.596 mS cm^{-1} respectively [24, 25]. If these measurements are taken as an approximation of bulk intracellular conductivity, then they correspond to a longitudinal diffusion coefficient $D_{||}$ of between 0.174 and $0.344 \text{ mm}^2 \text{ ms}^{-1}$, and a transverse diffusion coefficient D_{\perp} of between 0.0193 and $0.0596 \text{ cm}^2 \text{ ms}^{-1}$ for C_m of $1 \mu\text{F cm}^{-2}$ and S_v of 1000 cm^{-1} [23]. In practice, values of $D_{||}$ and D_{\perp} are typically chosen to match measured values of plane wave propagation speed along and across fibres. In cardiac ventricular tissue, measurements of longitudinal conduction velocity are typically between 0.4 and 0.6 ms^{-1} along fibres, and measurements of transverse conduction velocity are around half this value [26]. The diffusion coefficient determines the conduction velocity, which is proportional to the square root of bulk conductance [27, 28]. A 1:2 ratio of conduction velocity therefore implies a 1:4 ratio of diffusion coefficient. However, the anisotropy ratio used in simulation studies of re-entry has ranged from 1:1 (isotropic diffusion) to 1:4 [15, 29, 30], 1:5 [17, 18, 22, 31], around 1.5 [32], and 1:9 [33-37].

In this study $D_{||}$ was set to either 0.1 or $0.2 \text{ mm}^2 \text{ ms}^{-1}$ and D_{\perp} to either 0.025 or $0.05 \text{ mm}^2 \text{ ms}^{-1}$. These values were used in five combinations with anisotropy ratios of 1:4, 1:2, 1:4, 1:8, and 1:1; 0.1 and $0.025 \text{ mm}^2 \text{ ms}^{-1}$, 0.1 and $0.05 \text{ mm}^2 \text{ ms}^{-1}$, 0.2 and $0.025 \text{ mm}^2 \text{ ms}^{-1}$, 0.2 and $0.05 \text{ mm}^2 \text{ ms}^{-1}$, and 0.1 and $0.1 \text{ mm}^2 \text{ ms}^{-1}$. The largest and smallest diffusion coefficients of $D_{||}=0.2$ and

$D_{\perp}=0.025 \text{ mm}^2\text{ms}^{-1}$ gave plane wave conduction velocities of 0.75 ms^{-1} parallel to fibres and 0.21 ms^{-1} orthogonal to fibres.

Numerical scheme

Equation (1) was solved using a finite difference implementation described in detail elsewhere [38], which used an explicit Euler scheme with a fixed time step of 0.05 ms, and a fixed space step of 0.25 mm. All computations used double precision arithmetic, with no-flux boundary conditions imposed at each surface. A change in plane wave conduction velocity of less than 5.5% was observed with time steps of 0.04 and 0.06 ms for $D_{\parallel}=0.2 \text{ mm}^2\text{ms}^{-1}$, and was lower for the other values of diffusion coefficient, indicating stability of the numerical scheme for the combination of time and space step, and for the diffusion ratios used in this study.

Tissue geometry

Fibrillation was simulated in a rectilinear slab, with dimensions of $79.5 \times 79.5 \times 13$ mm ($318 \times 318 \times 52$ grid points). The slab was designed to reflect part of the mammalian left ventricular wall. Fibres were aligned parallel to the top and bottom surfaces, with a linear transmural fibre rotation giving a total change in orientation of 120° between the top and bottom surfaces.

Since conduction velocity is proportional to the square root of the diffusion coefficient, the effective size of the tissue geometry varied with the different values of D_{\parallel} and D_{\perp} . We estimated the effective size of the tissue relative to simulations with of $D_{\parallel}=D_{\perp}=0.1 \text{ mm}^2\text{ms}^{-1}$, so that for $D_{\parallel}=0.2$ and $D_{\perp}=0.05 \text{ mm}^2\text{ms}^{-1}$ the effective size of the tissue was given by

$$318\sqrt{2} \times \frac{318}{\sqrt{2}} \times \frac{52}{\sqrt{2}} = 318 \times 318 \times 52 \times \frac{1}{\sqrt{2}}.$$

These measures of effective size enabled a rough comparison of the numbers of filaments and PS in the simulations with different anisotropic ratios. However, two important points should be noted. First, the rotational anisotropy used in this study means that the effective geometries of simulations with different anisotropy were not directly comparable, notwithstanding the use of effective size. Second, although the use of effective size enabled the influence of anisotropy ratio on filament dynamics to be assessed independent of tissue size, the influence of anisotropy ratio on filament dynamics in tissue of fixed absolute size is also an important and separate question.

Initial conditions

Re-entry was initiated using the phase distribution technique [39]. Stacked spiral waves were imposed on the tissue as an initial condition to produce an untwisted scroll wave filament linking the top and bottom faces. The filament was tilted by 71° to the transmural direction, as pilot simulations showed that this promoted filament breakup and multiple wavelet fibrillation by reducing the effects of positive filament tension. This filament connected the large faces of the slab, and hence represented a filament that would have a transmural alignment in the ventricle.

Detecting phase singularities and filaments

Filaments can be detected using the intersection of isosurfaces of membrane voltage V_{iso} , and $dV_m/dt = 0$ [17, 40]. However, this approach is very sensitive to the choice of V_{iso} [41], and so for the present study a method based on phase space analysis was used [38, 42]. We transformed membrane voltage into phase using time delay embedding with a delay of 4 ms. The origin of the phase space trajectory was set to the mean values of V_m and time delayed V_m , except when these mean values dropped below a threshold of -75 mV, where the origin coordinate was set to -60 mV. Voxels containing filaments were identified using

convolution kernels [43], and a smoothing algorithm based on a 3x3x3 boxcar filter was then used to ensure the filaments were continuous. Continuous filaments were then identified and tagged using a grassfire algorithm. This process is illustrated in Figure 3.

Tracking phase singularities and filaments

Snapshots of the tagged filaments were retained at 2 ms intervals, and individual filaments were tracked by identifying overlap of filament voxels from one snapshot to the next. This approach enabled filament births, deaths, divisions, and amalgamations to be identified [40]. A single filament may interact with many others through division and amalgamation events, and so the lifetime of a particular filament is ambiguous. Hence in this study the time interval between interaction events was determined, and this index was used to describe filament lifetime [15].

Surface PS were tagged and tracked from the top ($z = 0$) layer of the simulated tissue, using the same 2 ms snapshots as used for filaments. A two stage approach was used. First, a search radius of 1 mm was used to link PS from one snapshot to the next. PSs that did not lie within the search radius were then tagged as having died or having been born. In the second analysis stage, these birth and death events were refined, to take account of rapidly moving PS. Hence if a PS birth and PS death were associated with the same filament tag, and occurred within 3 mm of each other then they were considered to be a rapidly moving surface PS. This tracking information was used to record an estimate of PS lifetime, and the number of PS associated with each filament.

Given these definitions, in this study a single surface PS occurred when a filament touched the surface. A single PS could persist while its associated filament amalgamated or divided, and in this case the PS lifetime would be longer than the

filament lifetime. Conversely a single filament could be associated with several occurrences of a PS as the filament moved within the tissue to touch the top surface, then the side, and then the top surface again.

Results

Number of filaments

Figure 4a shows how the number of filaments changed during time in each simulation. In each case, the single transmural filament imposed as the initial condition fragmented, resulting in many interacting filaments. Figure 4b shows a moving average of Figure 4a, calculated using a 100 ms sliding window. Example snapshots of the filaments 100, 400, and 900 ms after initiation are shown in Figure 4d for $D_{||}=0.1$ and $D_{\perp}=0.1 \text{ mm}^2\text{ms}^{-1}$ and in Figure 4e for $D_{||}=0.2$ and $D_{\perp}=0.025 \text{ mm}^2\text{ms}^{-1}$. For the isotropic simulation with $D_{||}=0.1$ and $D_{\perp}=0.1 \text{ mm}^2\text{ms}^{-1}$, the re-entrant activity self terminated after 1176 ms. In all of the other simulations the number of filaments increased during an initial period up to 1000 ms, and then settled down to fluctuate around a mean value.

Figure 4a shows a larger number of filaments in the simulations with $D_{\perp}=0.025 \text{ mm}^2\text{ms}^{-1}$ compared to the others, with the lowest number of filaments observed in the isotropic simulation with $D_{||}=0.1$ and $D_{\perp}=0.1 \text{ mm}^2\text{ms}^{-1}$. These data indicate that the transverse component of diffusion has an important effect on the complexity of multiple wavelet re-entry. This observation is supported by Figure 4d and 4e. In Figure 4d $D_{||}=0.1$ and $D_{\perp}=0.1 \text{ mm}^2\text{ms}^{-1}$, and most of the filaments in these snapshots are aligned transmurally, linking the top and bottom surfaces. Throughout this isotropic simulation the mean proportion of transmural filaments was 0.72 (SD=0.21). In contrast, Figure 4e shows snapshots for $D_{||}=0.2$ and $D_{\perp}=0.025 \text{ mm}^2\text{ms}^{-1}$, and there are not only more filaments present compared to the snapshots in Figure 4d, but there is a greater intramural

component to their orientation. Throughout this anisotropic simulation the mean proportion of transmural filaments was 0.40 (SD=0.18). For the other anisotropic simulations with $D_{||}$ and D_{\perp} set to 0.1 and 0.025 $\text{mm}^2\text{ms}^{-1}$, 0.1 and 0.05 $\text{mm}^2\text{ms}^{-1}$, and 0.2 and 0.05 $\text{mm}^2\text{ms}^{-1}$, the mean proportion of transmural filaments was 0.36 (SD=0.18), 0.53 (SD=0.18), and 0.53 (SD=0.19). The mean proportion of ring filaments for simulations with $D_{||}$ and D_{\perp} set to 0.1 and 0.025 $\text{mm}^2\text{ms}^{-1}$, 0.1 and 0.05 $\text{mm}^2\text{ms}^{-1}$, 0.2 and 0.05 $\text{mm}^2\text{ms}^{-1}$, 0.1 and 0.025 $\text{mm}^2\text{ms}^{-1}$, and 0.2 and 0.025 $\text{mm}^2\text{ms}^{-1}$ was 0.01 (SD=0.03), 0.02 (SD=0.05), 0.02 (SD=0.05), 0.07 (SD=0.07), and 0.06 (SD=0.06). These observations indicate that higher values of transverse diffusion coefficient are associated with more transmural and fewer ring filaments.

Figure 4c shows the number of filaments in each simulation adjusted for the effective size of tissue geometry. In this case there was less difference between the numbers of filaments observed for each anisotropy ratio, indicating a similar density of filaments in each simulation, once differences in conduction velocity resulting from the different anisotropy ratio were taken into account. This observation is consistent to the finding in a previous study using a biophysically and anatomically detailed model of VF in the human heart [15]

Proportion of filaments visible on surface

A single filament may intersect the tissue surface as a PS zero or more times. Figure 5a shows the number of PS and Figure 5b the number of PS per filament for each simulation. Table 2 summarises the numbers of filaments and PS for each simulation, both for the entire simulation, and also for the period from 1000-2000 ms when the number of filaments and PS was quasi-stable. The numbers of PS followed the same overall pattern as the number of filaments, being elevated for the simulations with $D_{\perp}=0.025 \text{ mm}^2\text{ms}^{-1}$. The numbers of PS were slightly lower than the number of filaments, with an average number of PS

per filament of between 0.82 and 0.93. Transverse diffusion had a small effect, with lower transverse diffusion resulting in a larger number of PS per filament.

Lifetime of filaments and surface phase singularities

Figure 6 summarises the lifetimes of filaments and phase singularities observed in this study. In Figures 6a and 6c the horizontal lines record the lifetime of each filament and PS, using an idea taken from a recent study of simulated VF in the human heart [15]. For a filament, the lifetime was defined as the interval between a creation event (birth, division or amalgamation) and an annihilation event (death, amalgamation or division). For a PS, lifetime was defined as the interval between birth and death.

Overall, PS were much longer lived than filaments. This is emphasised by the data in Table 3, which indicate that the longest lived PS persisted for more than half of the simulation. Transverse diffusion influenced PS lifetime, and lower values of transverse diffusion were associated with a higher maximum PS lifetime, although the median lifetime was broadly similar for each anisotropy ratio. However, this trend was not apparent for the filament lifetimes. Figures 6b and 6d show the distribution of filament and PS lifetimes respectively, and indicate that despite the long tail, the majority of filaments and PS were relatively short-lived, and this profile of lifetimes is in agreement with data from other computational and experimental studies [15, 44].

Creation and annihilation of filaments and surface phase singularities

Figure 7a and 7b show the creation and annihilation of filaments plotted against the number of filaments present. The creation and annihilation rates were estimated by binning the number of filaments created (births + divisions) and annihilated (deaths + amalgamations) by the number of filaments (NF). The rate of creation (and annihilation) was then estimated as the mean number of created

(and annihilated) filaments corresponding to each NF. Figures 7d and 7e show the corresponding data for surface PS.

Overall these data indicate that anisotropy ratio has little effect on the relationship between creation, annihilation and the number of filaments and PS. Furthermore these data also show that the creation and annihilation rate for both filaments and PS in the model used in the present study is a linear function of the number of filaments and PS respectively.

The number of filaments and PS did not appear to influence the difference between creation and annihilation rate (Figures 7c and 7f). Overall, the mean difference between creation and annihilation rate was 0.019 (SD=0.545) for filaments, and 0.143 (SD=0.492) for PS. This slight excess of creation over annihilation accounts for the increasing numbers of PS and filaments during the early phase of simulated VF.

Discussion

The main findings of this computational study are as follows:

- Anisotropy ratio influenced the number of filaments sustaining simulated VF, with more filaments present in simulations with smaller values of transverse diffusion coefficient.
- When the size of the slab geometry was adjusted for changes in conduction velocity arising from different values of the transverse diffusion coefficient, the number of filaments in each simulation was comparable.
- Each re-entrant filament was associated with around 0.9 PS on the top surface of the slab geometry used in this study. The anisotropy ratio exerted a small influence on this quantity, with a smaller transverse diffusion coefficient being associated with more PS per filament.

- PS were much longer lived than filaments, and a small number of PS had lifetimes of up to 1 s. Anisotropy ratio had no effect on filament lifetime, but maximum PS lifetimes were longer for simulations with smaller transverse diffusion coefficient.
- The creation and annihilation of filaments and PS were linear functions of the number of filaments and PS, and these relationships were independent of the anisotropy ratio.

Anisotropy, and importance of transverse diffusion coefficient

This study has shown that in a simplified computational model, the anisotropy of cardiac tissue plays an important role in determining the complexity of VF sustained by multiple wavelet re-entry. Anisotropy influenced the number of filaments, the number of surface PS, the proportion of filaments that are manifest as a surface PS, and the lifetime of the longest lived surface PS. In each case, the magnitude of the transverse diffusion coefficient had a greater influence than the anisotropy ratio.

In the slab geometry used in this study, the transverse diffusion coefficient determines the effective thickness of the slab. Figure 4c indicates that this effect accounts for much of the difference in the number of filaments observed in the simulations with different transverse diffusion coefficient. The greater effective thickness also accounts for the lower proportion of transmural filaments observed in the simulations with lower transverse diffusion coefficient.

Filaments that are not aligned transmurally are, by definition, less likely associated with a surface PS. Moreover, intramural filaments may tend to align themselves with fibres [33]. Hence we would expect a lower transverse diffusion coefficient, associated with fewer transmural filaments, to also be associated with

a smaller number of PS per filament. This was not the case, and the average number of PS per filament was slightly higher for the simulations with the lowest transverse diffusion coefficient. One explanation for this observation is that for lower values of transverse diffusion, U shaped filaments, associated with two surface PS, predominate rather than fully intramural filaments. This explanation is supported by the higher proportion of ring filaments observed in the simulations with smaller transverse diffusion coefficient, since ring filaments readily form U shaped filaments if they move close to a surface. However, the small numbers of ring filaments observed do indicate that filament interactions tend to destabilise rings once they form. This constant interaction of filaments may also counteract the tendency to align with fibre direction, although more studies are needed to establish whether this is the case.

There remain a number of unanswered questions about anisotropy in the ventricular wall. First, this study has assumed that the anisotropy ratio is constant throughout the ventricular wall, and that the rotation of fibres is a linear function of transmural distance. These assumptions may not be correct, especially in the whole heart. Experimental data indicate that the expression of cardiac gap junction proteins across the ventricular wall is both non-uniform[45] and influenced by disease [46], and even early studies of fibre rotation indicated that fibre rotation rate may not be constant [47]. Second, there is mounting evidence that the orthotropic (fibre-sheet) anisotropy of cardiac tissue may play a role in action potential propagation [48], with a recent study indicating that the electrical properties of cardiac tissue are best described by conductivities in the fibre direction, and parallel and normal to sheets in the ratio 4:2:1 [49]. Finally, this study used a greatly simplified geometrical model of the ventricle wall. Anatomically detailed geometries are available, and have been used for whole ventricle simulation studies of VF in rabbit [50], dog [29, 30, 32, 51] and human [15] geometry. These geometrical datasets have been obtained from small

numbers of individuals [52, 53], and so may not represent the range of anisotropy present in populations of real hearts, especially when the effects of disease are considered. However, new imaging modalities such as diffusion tensor MRI [54, 55], and high resolution MRI [56] can be expected to establish the variability of anatomy and anisotropy between individuals.

Surface manifestation of filaments

In this study we found that the average number of PS per filament was around 0.9. This is higher than the value of around 0.7 observed for whole ventricle geometry [15]. The present study used simplified slab geometry, whereas the ventricles have two chambers separated by a septum. Hence, a lower number of PS per filament would be expected for the anatomically detailed geometry, because the ratio of tissue volume to surface area is larger.

PS and filament lifetimes

This study found that PS lifetimes were longer than filament lifetimes, and one possible explanation is the definition chosen for filament lifetime. A single PS could persist while its associated filament amalgamated or divided, resulting in a PS lifetime that was longer than the filament lifetime. This is a consequence of the ambiguity of filament lifetime; when a filament divides, does the filament identity persist in one or more of its children, or are all of the children to be treated as new entities? From an experimental perspective, one group has proposed the notion of a compound rotor [44], where several short-lived PS are treated as the same entity. Although this approach may be more useful in the analysis of noisy experimental data, where transient wavefront block and fragmentation may occur close to the surface, it may also prove useful in quantifying simulation data because it attempts to distinguish between short lived wavebreak and persistent rotors. Another possible explanation for longer PS lifetimes compared to filament lifetimes is greater stability and longevity of

transmural filaments compared to non-transmural filaments. More studies are needed to address this question in detail.

The long PS lifetimes observed in the present study are in quantitative agreement with findings from other experimental [57] and computational [15] studies, where surface PS that persisted for more than 1 s were observed. One mechanism that could sustain VF is a mother rotor [58], where a single, rapidly rotating re-entrant wave enslaves the surrounding tissue. This is distinct from the multiple wavelet mechanism, where re-entrant waves are continually created and annihilated [59]. The hallmarks of a mother rotor are its persistence, high frequency, and spatial localisation. In this study, VF was sustained by the multiple-wavelet mechanism, mediated by steep APD restitution. Since the dynamic properties of the simulated tissue were homogenous, we would not expect the formation of a high-frequency mother rotor. Nevertheless, Figure 8 shows that the long lasting PS observed in this study tended to remain in a small area, indicating that multiple-wavelet VF may have some of the hallmarks of mother rotor VF.

Creation and annihilation

A theoretical and numerical study of PS dynamics in 2D systems proposed a constant creation rate, with an annihilation rate depending on the square of the number of PS [60]. A recent computational study in a 3D cube geometry [61] showed that the creation and annihilation of surface PS associated with 3D filaments did not fit this model. Instead, PS creation rate was proportional to the number of PS, and the annihilation rate was proportional to the square of the number of PS as well as a linear term. This difference could not be accounted for by either boundary effects, noise, or strong correlations between PS [61]. The findings of the present study confirm that in 3D systems the creation rate of surface PS is not constant, but rather is a linear function of the number of PS. We

have also shown a similar behaviour for filaments, and have shown that this relationship is independent of the anisotropy ratio. We also found a linear dependence of annihilation rate of PS and filaments on the number of PS and filaments respectively. It is possible that for the system investigated in the present study, the instability mechanism results in a small coefficient for the quadratic term found in the previous study [61]. Another possible explanation for the difference is the thin slab geometry used in the present study. Further work with different instability mechanisms will enable the mechanisms that are important for VF in the heart to be established. It will also be important to consider the role of slab thickness and the influence of anatomically detailed cardiac ventricular geometry on these dynamics.

Limitations

The findings of this study must be considered in the light of three important limitations. First, the specific computational model used in the study included simplified descriptions of cell and tissue electrophysiology, as well as idealised tissue geometry. In the model used in this study, the predominant mechanism sustaining VF was instability arising from steep APD restitution. Several other mechanisms could sustain VF in real cardiac tissue, and these mechanisms would be expected to influence filament and PS dynamics [18]. Biophysically detailed models of cardiac cellular electrophysiology have been developed for a number of different species, and capture the detailed behaviour of ion channels, pumps and exchangers in the cell membrane as well as intracellular Ca^{2+} storage and release [62]. However, these more detailed models should be used with care because their behaviour in tissue is not always predictable [63]. Simulations using the more detailed bidomain model of tissue have also shown that boundary conditions may be important [64], and the detailed role played by geometry remains incompletely understood. Second, this study has ignored the influence of

mechanics. Initial modelling studies have shown that although the contraction of cardiac tissue during VF is small relative to contraction during a normal beat, mechanics does influence the behaviour of re-entrant waves [65, 66]. Finally, as well as being greatly simplified, the computational model used in this study was also generic, and cannot be directly used to infer the properties of VF in the heart of any particular species. However, despite this limitation there is a broad agreement between the findings of the present study and those of another recent study that used a detailed model of the human ventricle [15], indicating that the overall influence of anisotropy on VF dynamics is robust between species and models.

Implications and further work

This study has two main implications for our understanding of the mechanisms that sustain VF in the heart. First, the findings of the present study emphasise that the mechanisms that sustain fibrillation in the 3D thick-walled ventricle are quantitatively different from those that sustain fibrillation in 2D simulations and in the thin-walled atria. Not all filaments are manifest as surface PS, and the lifetimes and interaction dynamics of filaments are different from those of PS. Hence, although 2D simulations are a valuable tool for investigating properties and mechanisms of re-entry, caution should be exercised in extending findings from 2D simulations to 3D tissue. Second, anisotropy has an important influence on the complexity of multiple-wavelet VF.

Further studies are needed to establish how geometry and wall thickness determine the proportion of filaments that are visible as a surface PS, and how this relationship may be influenced by transmural differences in action potential shape and duration, nonlinear changes in diffusion across the ventricular wall, and the choice of simplified and biophysically detailed cell models.

Acknowledgements

The computations and analysis presented here were done in part using machines on the White Rose Grid (<http://www.wrgrid.org.uk/>), and in part on in the University of Leeds Computational Biology Laboratory kindly made available by Professor Arun Holden. I am also grateful for support from the Integrative Biology eScience project (EPSRC Grant No. GR/572023/01) and the British Heart Foundation (Grant numbers BS 98001 and PG/03/102/1582).

References

- [1] R. E. Ideker, G. J. Klein, L. Harrison, W. M. Smith, J. Kasell, K. A. Reimer, A. G. Wallace, and J. J. Gallagher, "The transition to ventricular fibrillation induced by reperfusion after acute regional ischaemia in the dog: A period of organised epicardial activation," *Circulation*, vol. 63, pp. 1371-1379, 1981.
- [2] M. Nash, A. Mourad, R. Clayton, P. Sutton, C. Bradley, M. Hayward, D. Paterson, and P. Taggart, "Evidence for multiple mechanisms in human ventricular fibrillation.," *Circulation.*, vol. 114, pp. 536-42, 2006.
- [3] J. M. Davidenko, A. V. Pertsov, R. Salomonsz, W. Baxter, and J. Jalife, "Stationary and Drifting Spiral Waves of Excitation in Isolated Cardiac-Muscle," *Nature*, vol. 355, pp. 349-351, 1992.
- [4] F. X. Witkowski, L. J. Leon, P. A. Penkoske, W. R. Giles, M. L. Spano, W. L. Ditto, and A. T. Winfree, "Spatiotemporal evolution of ventricular fibrillation," *Nature*, vol. 392, pp. 78-82, 1998.
- [5] R. A. Gray, A. M. Pertsov, and J. Jalife, "Spatial and temporal organization during cardiac fibrillation," *Nature*, vol. 392, pp. 75-78, 1998.
- [6] I. R. Efimov, V. Sidorov, Y. Chen, and B. Wollenzier, "Evidence of three-dimensional scroll waves with ribbon filaments as a mechanism of ventricular tachycardia in the isolated rabbit heart," *Journal of Cardiovascular Electrophysiology*, vol. 10, pp. 1452-1462, 1999.
- [7] A. Pertsov, "Scroll waves in three dimensions," in *Cardiac electrophysiology from cells to bedside*, J. Jalife and D. P. Zipes, Eds., 4 ed. Philadelphia: Saunders, 2004, pp. 345-354.
- [8] M. J. Bishop, B. Rodriguez, J. C. Eason, J. P. Whiteley, N. Trayanova, and D. J. Gavaghan, "Synthesis of voltage-sensitive optical signals: application to panoramic optical mapping," *Biophysical Journal*, vol. 90, pp. 2938-2945, 2006.
- [9] W. T. Baxter, S. F. Mironov, A. V. Zaitsev, J. Jalife, and A. M. Pertsov, "Visualizing excitation waves inside cardiac muscle using transillumination," *Biophysical Journal*, vol. 80, pp. 516-530, 2001.
- [10] M. Wellner, O. Bernus, S. F. Mironov, and A. M. Pertsov, "Multiplicative optical tomography of cardiac electrical activity," *Physics in Medicine and Biology*, vol. 51, pp. 4429-4446, 2006.
- [11] A. T. Winfree, *The geometry of biological time*, 2nd ed. New York: Springer-Verlag, 2000.
- [12] R. H. Clayton, E. A. Zhuchkova, and A. Panfilov, "Phase singularities and filaments: Simplifying complexity in computational models of ventricular

- fibrillation.," *Progress in Biophysics and Molecular Biology*, vol. 90, pp. 378-398, 2006.
- [13] J. Rogers, J. Huang, S. Melnick, and R. Ideker, "Sustained reentry in the left ventricle of fibrillating pig hearts.," *Circulation research.*, vol. 92, pp. 539-45, 2003.
- [14] J. M. Rogers, J. Huang, W. M. Smith, and R. E. Ideker, "Incidence, evolution, and spatial distribution of functional reentry during ventricular fibrillation in pigs," *Circulation Research*, vol. 84, pp. 945-954, 1999.
- [15] K. H. W. J. TenTusscher, R. Hren, and A. V. Panfilov, "Organization of ventricular fibrillation in the human heart," *Circulation Research*, vol. 100, pp. e87-e101, 2007.
- [16] I. J. LeGrice, B. H. Smaill, L. Z. Chai, S. G. Edgar, J. B. Gavin, and P. J. Hunter, "Laminar structure of the heart: ventricular myocyte arrangement and connective tissue architecture in the dog," *American Journal of Physiology (Heart and Circulatory Physiology)*, vol. 269, pp. 571-82, 1995.
- [17] F. Fenton and A. Karma, "Vortex dynamics in three-dimensional continuous myocardium with fibre rotation: Filament instability and fibrillation," *Chaos*, vol. 8, pp. 20-47, 1998.
- [18] F. H. Fenton, E. M. Cherry, H. M. Hastings, and S. J. Evans, "Multiple mechanisms of spiral wave breakup in a model of cardiac electrical activity," *Chaos*, vol. 12, pp. 852-892, 2002.
- [19] R. H. Clayton and P. Taggart, "Regional differences in APD restitution can initiate wavebreak and re-entry in cardiac tissue: A computational study," *Biomedical Engineering OnLine*, vol. 4, pp. 54, 2005.
- [20] R. H. Clayton and A. V. Holden, "Dynamics and interaction of filaments in a computational model of re-entrant ventricular fibrillation," *Physics in Medicine and Biology*, vol. 47, pp. 1777-1792, 2002.
- [21] R. A. Oliver and W. Krassowska, "Reproducing cardiac restitution properties using the Fenton-Karma membrane model," *Annals of Biomedical Engineering*, vol. 33, pp. 907-911, 2005.
- [22] Z. L. Qu, K. Kil, F. G. Xie, A. Garfinkel, and J. N. Weiss, "Scroll wave dynamics in a three-dimensional cardiac tissue model: Roles of restitution, thickness, and fiber rotation," *Biophysical Journal*, vol. 78, pp. 2761-2775, 2000.
- [23] M. Potse, B. Dube, J. Richer, A. Vinet, and R. M. Gulrajani, "A comparison of monodomain and bidomain reaction-diffusion models for action potential propagation in the human heart," *IEEE Transactions on Biomedical Engineering*, vol. 53, pp. 2425-2435, 2006.
- [24] J. Malmivuo and R. Plonsey, *Bioelectromagnetism. Principles and applications of bioelectric and biomagnetic fields.*, 1st ed. New York: Oxford University Press, 1995.
- [25] B. J. Roth, "Electrical conductivity values used with the bidomain model of cardiac tissue," *IEEE Transactions on Biomedical Engineering*, vol. 44, pp. 326-328, 1997.
- [26] A. G. Kleber and Y. Rudy, "Basic mechanisms of cardiac impulse propagation and associated arrhythmias," *Physiological Reviews*, vol. 84, pp. 431-488, 2004.
- [27] A. L. Hodgkin, "A note on conduction velocity," *Journal of Physiology*, vol. 125, pp. 221-224, 1954.
- [28] M. K. Walton and H. A. Fozzard, "The conducted action potential: models and comparison to experiments," *Biophysical Journal*, vol. 44, pp. 9-26, 1983.
- [29] R. H. Clayton and A. V. Holden, "Filament behaviour in a computational model of ventricular fibrillation in the canine heart," *IEEE Transactions on Biomedical Engineering*, vol. 51, pp. 28-34, 2004.

- [30] F. Xie, Z. L. Qu, J. Yang, A. Baher, J. N. Weiss, and A. Garfinkel, "A simulation study of the effects of cardiac anatomy in ventricular fibrillation," *Journal of Clinical Investigation*, vol. 113, pp. 686-693, 2004.
- [31] W.-J. Rappel, "Filament instability and rotational anisotropy: A numerical study using detailed cardiac models," *Chaos*, vol. 11, pp. 71-80, 2001.
- [32] O. Berenfeld and J. Jalife, "Purkinje-muscle reentry as a mechanism of polymorphic ventricular arrhythmias in a 3-dimensional model of the ventricles," *Circulation Research*, vol. 82, pp. 1063-1077, 1998.
- [33] O. Berenfeld and A. M. Pertsov, "Dynamics of intramural scroll waves in three-dimensional continuous myocardium with rotational anisotropy," *Journal of Theoretical Biology*, vol. 199, pp. 383-394, 1999.
- [34] O. Wellner, O. Berenfeld, J. Jalife, and A. Pertsov, "Minimal principle for rotor filaments," *Proceedings of the National Academy of Sciences*, vol. 99, pp. 8015-8018, 2002.
- [35] R. L. Winslow, D. F. Scollan, J. L. Greenstein, C. K. Yung, W. Baumgartner Jr, G. Bhanot, D. L. Gresh, and B. E. Rogowitz, "Mapping, modeling, and visual exploration of structure-function relationships in the heart," *IBM Systems Journal*, vol. 40, pp. 342-359, 2001.
- [36] A. V. Panfilov and J. P. Keener, "Generation of reentry in anisotropic myocardium," *Journal of Cardiovascular Electrophysiology*, vol. 4, pp. 412-421, 1993.
- [37] A. V. Panfilov and J. P. Keener, "Re-entry in three-dimensional Fitzhugh-Nagumo medium with rotational anisotropy," *Physica D*, vol. 84, pp. 545-552, 1995.
- [38] R. H. Clayton and A. V. Panfilov, "A guide to modelling cardiac electrical activity in anatomically detailed ventricles," *Progress in Biophysics & Molecular Biology*, pp. (in press), 2007.
- [39] V. N. Biktashev and A. V. Holden, "Re-entrant waves and their elimination in a model of mammalian ventricular tissue," *Chaos*, vol. 8, pp. 48-56, 1998.
- [40] R. H. Clayton and A. V. Holden, "A method to quantify the dynamics and complexity of re-entry in computational models of ventricular fibrillation," *Physics in Medicine and Biology*, vol. 47, pp. 225-238, 2002.
- [41] E. A. Zhuchkova and R. H. Clayton, "Methods for identifying and tracking phase singularities in computational models of re-entrant fibrillation," *Lecture Notes in Computer Science*, vol. 3504, pp. 246-255, 2005.
- [42] A. N. Iyer and R. A. Gray, "An experimentalist's approach to accurate localization of phase singularities during re-entry," *Annals of Biomedical Engineering*, vol. 29, pp. 47-59, 2001.
- [43] M.-A. Bray and J. P. Wikswo, "Use of topological charge to determine filament location and dynamics in a numerical model of scroll wave activity," *IEEE Transactions on Biomedical Engineering*, vol. 49, pp. 1086-1093, 2002.
- [44] M. W. Kay, G. P. Walcott, J. D. Gladden, S. B. Melnick, and J. M. Rogers, "Lifetimes of epicardial rotors in panoramic optical maps of fibrillating swine ventricles," *American Journal of Physiology (Heart and Circulatory Physiology)*, vol. 291, pp. H1935-H1941, 2006.
- [45] S. Poelzing, F. G. Akar, E. Baron, and D. S. Rosenbaum, "Heterogeneous connexin43 expression produces electrophysiological heterogeneities across the ventricular wall," *American Journal of Physiology (Heart and Circulatory Physiology)*, vol. 296, pp. H2001-H2009, 2004.
- [46] N. J. Severs, S. R. Coppin, E. Dupont, H.-I. Yeh, Y.-S. Ko, and T. Matsushita, "Gap junction alterations in human cardiac disease," *Cardiovascular Research*, vol. 62, pp. 368-377, 2004.
- [47] D. D. Streeter, "Gross morphology and fibrous structure of the heart," in *Handbook of Physiology - The Cardiovascular System*, vol. 1. Baltimore: American Physiological Society, 1979, pp. 61-112.

- [48] D. A. Hooks, K. A. Tomlinson, S. G. Marsden, I. J. LeGrice, B. H. Smaill, and A. Pullan, "Cardiac microstructure: Implications for electrical propagation and defibrillation in the heart," *Circulation Research*, vol. 91, pp. 331-338, 2002.
- [49] D. A. Hooks, M. L. Trew, B. J. Caldwell, G. B. Sands, I. J. LeGrice, and B. H. Smaill, "Laminar arrangement of ventricular myocytes influences electrical behavior of the heart.," *Circulation Research*, vol. 101, pp. DOI: 10.1161/CIRCRESAHA.107.161075, 2007.
- [50] B. Rodriguez, J. C. Eason, and N. Trayanova, "Differences between Left and Right Ventricular Anatomy Determine the Types of Reentrant Circuits Induced by an External Electric Shock. A Rabbit Heart Simulation Study," *Progress in Biophysics and Molecular Biology*, vol. 90, pp. 399-413, 2006.
- [51] A. V. Panfilov, "Three-dimensional organization of electrical turbulence in the heart," *Physical Review E*, vol. 59, pp. R6251-R6254, 1999.
- [52] P. M. F. Nielsen, I. J. E. LeGrice, B. H. Smaill, and P. J. Hunter, "Mathematical model of geometry and fibrous structure of the heart," *American Journal of Physiology (Heart and Circulatory Physiology)*, vol. 260, pp. H1365-H1378, 1991.
- [53] F. J. Vetter and A. D. McCulloch, "Three dimensional analysis of regional cardiac function: A model of rabbit ventricular anatomy," *Progress in Biophysics and Molecular Biology*, vol. 69, pp. 157-183, 1998.
- [54] D. F. Scollan, A. Holmes, J. Zhang, and R. L. Winslow, "Reconstruction of cardiac ventricular geometry and fibre orientation using magnetic resonance imaging," *Annals of Biomedical Engineering*, vol. 28, pp. 934-944, 2000.
- [55] P. Helm, M. Faisal, M. I. Miller, and R. L. Winslow, "Measuring and mapping cardiac fiber and laminar architecture using diffusion tensor imaging," *Annals of the New York Academy of Sciences*, vol. 1047, pp. 296, 2005.
- [56] R. A. B. Burton, G. Plank, J. E. Schneider, V. Grau, H. Ahammer, S. J. Keeling, J. Lee, N. P. Smith, D. Gavaghan, N. Trayanova, and P. Kohl, "3-Dimensional models of individual cardiac histo-anatomy: tools and challenges," *Annals of the New York Academy of Sciences*, vol. 1380, pp. 301-319, 2006.
- [57] S. M. Kaye and S. L. Marple, "Spectrum analysis - a modern perspective," *Proceedings of the IEEE*, vol. 69, pp. 1380-1419, 1981.
- [58] A. V. Zaitsev, O. Berenfeld, S. F. Mironov, J. Jalife, and A. M. Pertsov, "Distribution of excitation frequencies on the epicardial and endocardial surfaces of fibrillating ventricular wall of the sheep heart," *Circulation Research*, vol. 86, pp. 408-417, 2000.
- [59] J. M. Rogers and R. E. Ideker, "Fibrillating myocardium. Rabbit warren or beehive?," *Circulation*, vol. 86, pp. 369-370, 2000.
- [60] L. Gil, J. Lega, and J. L. Meunier, "Statstical properties of defect-mediated turbulence," *Physical Review A*, vol. 41, pp. 1138-1141, 1990.
- [61] M. Zhan, J. Davidsen, and R. Kapral, "Filament -induced surface spiral turbulence," (*personal communication*), 2007.
- [62] D. Noble and Y. Rudy, "Models of cardiac ventricular action potentials: iterative interaction between experiment and simulation," *Philosophical Transactions of the Royal Society of London Series A-Mathematical Physical and Engineering Sciences*, vol. 359, pp. 1127-1142, 2001.
- [63] E. M. Cherry and F. H. Fenton, "A tale of two dogs: Analyzing two models of canine ventricular electrophysiology," *American Journal of Physiology (Heart and Circulatory Physiology)*, pp. (in press), 2006.
- [64] A. Sambelashvilli and I. R. Efimov, "Dynamics of virtual electrode-induced scroll-wave reentry in a 3D bidomain model," *American Journal of Physiology (Heart and Circulatory Physiology)*, vol. 287, pp. H1570-H1581, 2004.

- [65] M. P. Nash and A. V. Panfilov, "Electromechanical model of excitable tissue to study reentrant cardiac arrhythmias," *Progress in Biophysics & Molecular Biology*, vol. 85, pp. 501-522, 2004.
- [66] A. V. Panfilov, R. H. Keldermann, and M. P. Nash, "Drift and breakup of spiral waves in reaction-diffusion-mechanics systems," *Proceedings of the National Academy of Sciences*, vol. 104, pp. 7922-7926, 2007.

Table 1. Parameter set for the 3V-SIM model.

Parameter	value	units
r		
t_d	0.25	ms
t_r	33.0	ms
t_{si}	30.0	ms
t_0	12.5	ms
t_v^+	3.33	ms
t_{v1}^-	19.6	ms
t_{v2}^-	1250.0	ms
t_w^+	870.0	ms
t_w^-	41.0	ms
u_c	0.13	None
u_v	0.05	None
u_c^{si}	0.85	None
k	10.0	None

Table 2. Summary data showing numbers of filaments and phase singularities throughout each simulation, and for the period between 1000 and 2000 ms.

Anisotropy ratio	Number of filaments					Number of PS					Mean PS per filament
	Overall		1000-2000 ms			Overall		1000-2000 ms			
	mean	SD	mean	SD	max	mean	SD	mean	SD	max	
01:0025	31.2	20.2	48.8	7.7	65	28.8	17.8	43.2	7.7	59	0.92
01:005	17.5	8.7	23.0	3.3	34	15.6	8.5	21.5	4.9	35	0.86
02:0025	32.3	20.6	49.8	6.7	64	31.0	19.2	46.1	7.4	66	0.93
02:005	17.6	8.9	22.9	4.2	32	14.7	7.7	20.0	4.1	31	0.82
01:01	5.1	2.5	---	---	11	4.7	2.7	---	---	11	0.89

Table 3. Summary data showing the lifetime of filaments and PS during each simulation.

Anisotropy ratio	Filament lifetime (ms)			PS lifetime (ms)		
	N	median	max	N	median	max
01:0025	2812	10	406	815	22	1010
01:005	1437	12	410	398	30	666
02:0025	3444	8	424	876	24	1242
02:005	1588	10	460	397	30	746
01:01	260	6	214	92	38	338

Figure captions

Figure 1. Example surface and 3D activation patterns during simulated re-entry in a slab of tissue. (a) 3D activation with a single re-entrant scroll wave. The isosurface encloses regions of electrical depolarisation with $V_m > -35$ mV. (b) Filament associated with the re-entrant wave shown in (a). This filament links the top and bottom surfaces of the simulated tissue. (c) Activation on the top surface of the slab. A single spiral wave can be seen, with a single phase singularity, shown by a star. (d) 3D activation with a multiple re-entrant scroll waves, that are interacting with each other. (e) Five filaments associated with the re-entrant waves shown in (d). (f) Activation on the top surface of the slab. Of the five filaments present in 3D, only three are manifest as surface phase singularities, and these are shown by stars.

Figure 2. Properties of the model used in this study. (a) Action potential duration and conduction velocity restitution obtained in 2D sheet with $D=0.1$ mm²ms⁻¹. (b) Snapshots of re-entry in 2D, showing the activation pattern 300, 500, 700, 900, and 1100 ms after initiation, with the same greyscale encoding of membrane voltage as in Figure 1. (c) Time series of V_m recorded from the upper left quadrant of the model.

Figure 3. Identification of filaments. (a) 3D activation in tissue slab, 500ms after initiation of re-entry. The isosurface encloses regions of electrical depolarisation with $V_m > -35$ mV. (b) Filament points extracted from voltage data using time delay embedding and phase transform (see text for details). (c) Connected filaments after spatial filtering of the data shown in (b). Shades of gray indicate filament tags.

Figure 4. Changes in the number of filaments over time. (a) Number of separate filaments identified in each simulation. (b) Number of filaments, smoothed using a moving average filter (see text for details). (c) Number of filaments, corrected for tissue size and anisotropy (see text for details). (d) Snapshots showing filaments in isotropic simulation with $D_{||}=0.1$ and $D_{\perp}=0.1$ mm²ms⁻¹, 100, 400 and 900 ms after initiation. (e) Snapshots showing filaments in anisotropic simulation with $D_{||}=0.1$ and $D_{\perp}=0.025$ mm²ms⁻¹, 100, 400 and 900 ms after initiation.

Figure 5. (a) Number of phase singularities, and (b) ratio of number of phase singularities to number of filaments, for each simulation.

Figure 6. Filament and phase singularity lifetimes. (a) Filament lifetime data, shown by drawing lines linking the time at which a filament was created and the time at which the filament was annihilated. (b) Histogram of filament lifetimes. (c) Phase singularity lifetime data, plotted in the same way as (a). (d) Histogram of phase singularity lifetimes.

Figure 7. Filament and phase singularity creation and destruction. (a) Filament creation rate plotted against number of filaments. (b) Filament annihilation rate plotted against number of filaments. (c) Difference between filament creation rate and annihilation rate plotted against number of filaments. (d) Phase singularity creation rate plotted against number of phase singularities. (e) Phase singularity annihilation rate plotted against number of phase singularities. (f) Difference between phase singularity creation rate and annihilation rate plotted against number of phase singularities.

Figure 8. Trajectory of longest lasting phase singularity on top surface of anisotropic simulation with $D_{||}=0.1$ and $D_{\perp}=0.025$ mm²ms⁻¹.

Figure 1

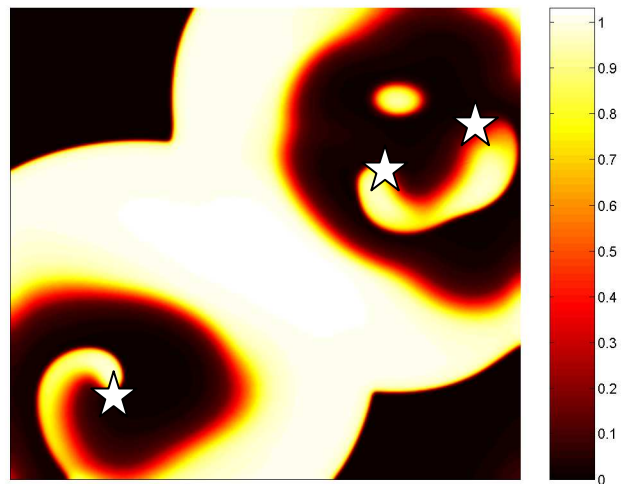
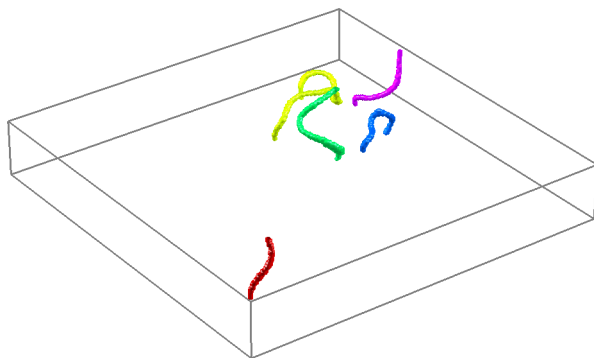
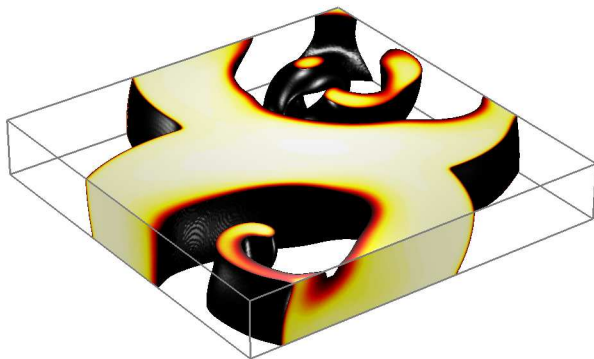
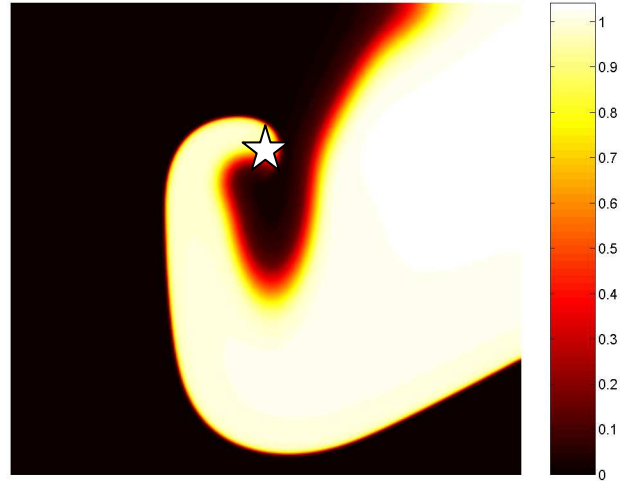
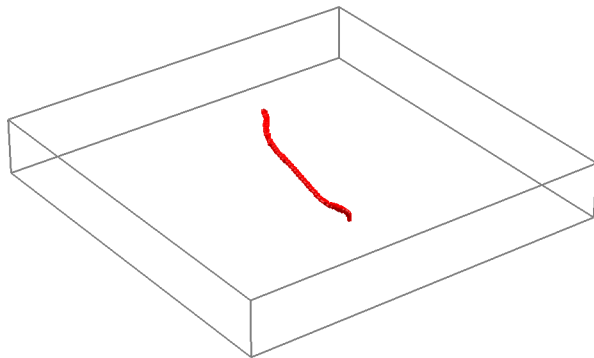
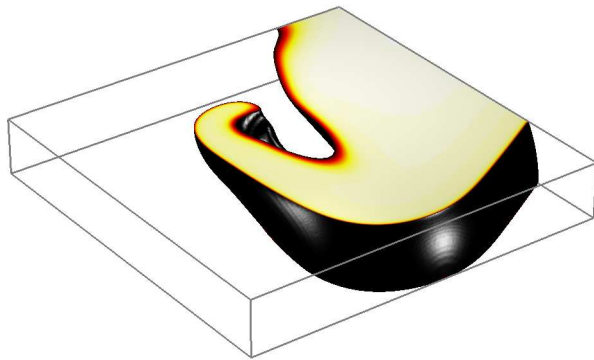


Figure 2

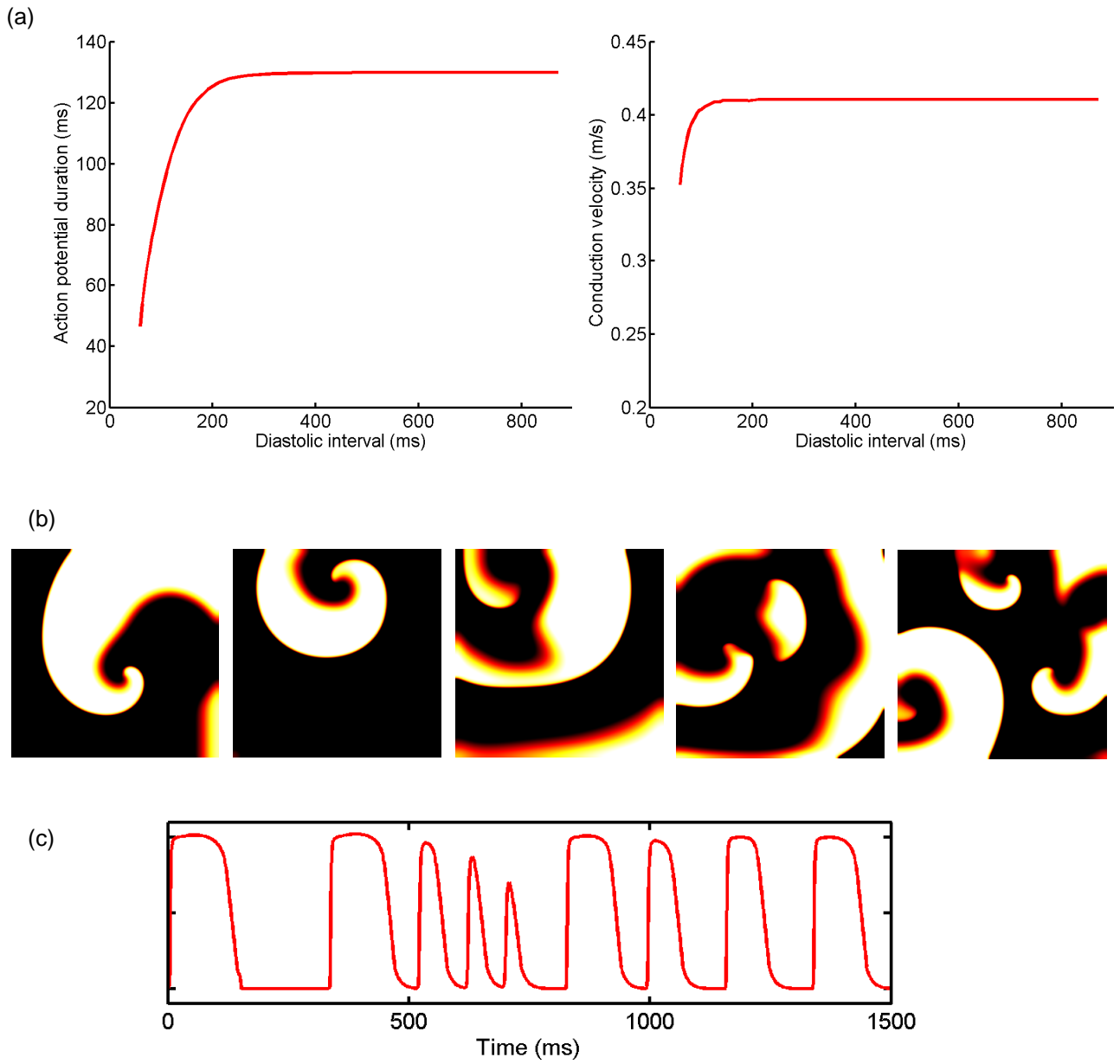
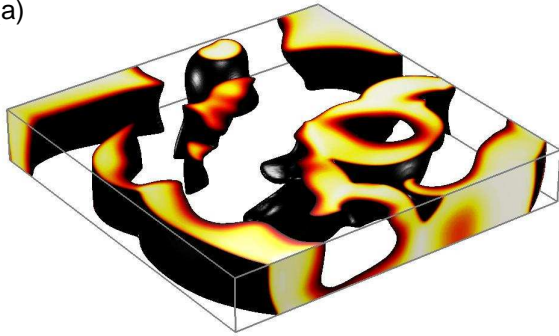
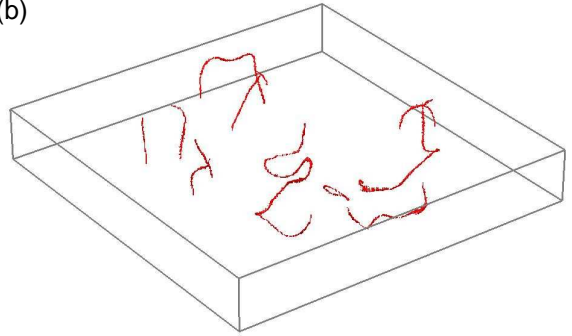


Figure 3

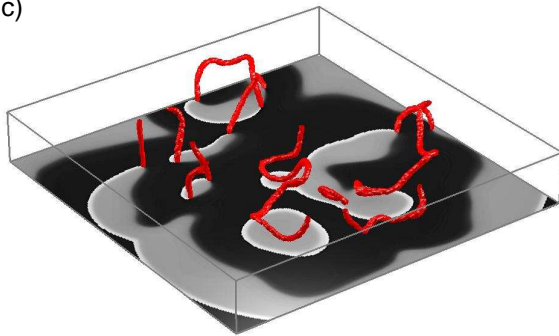
(a)



(b)



(c)



(d)

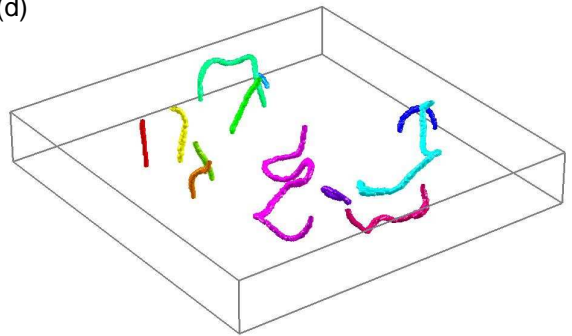
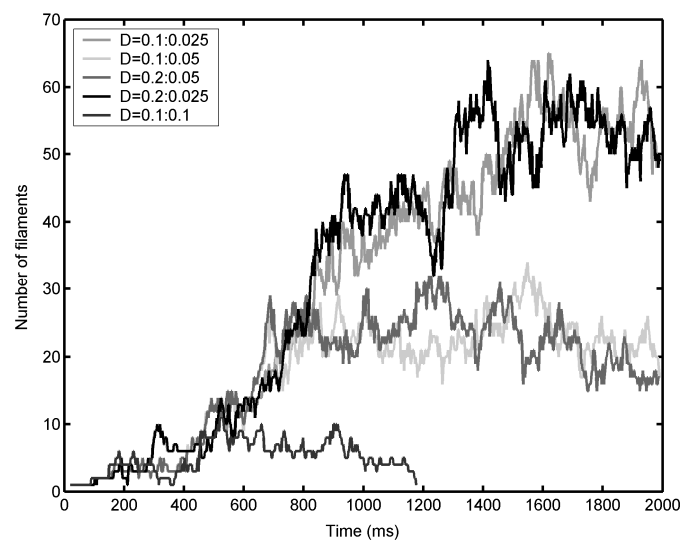
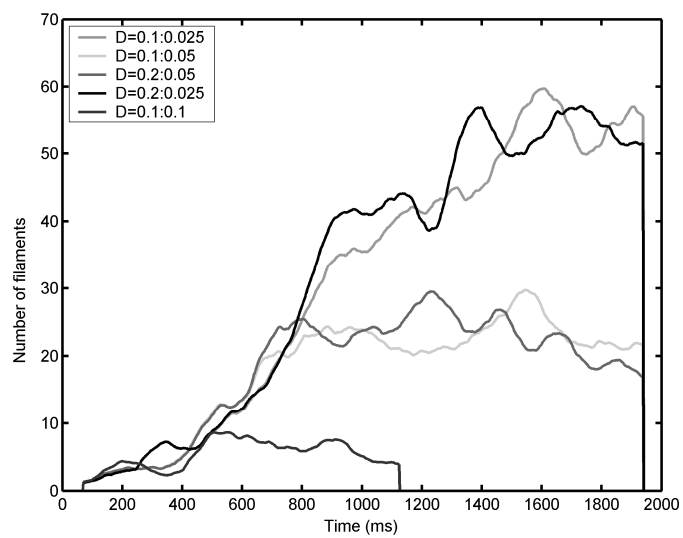


Figure 4

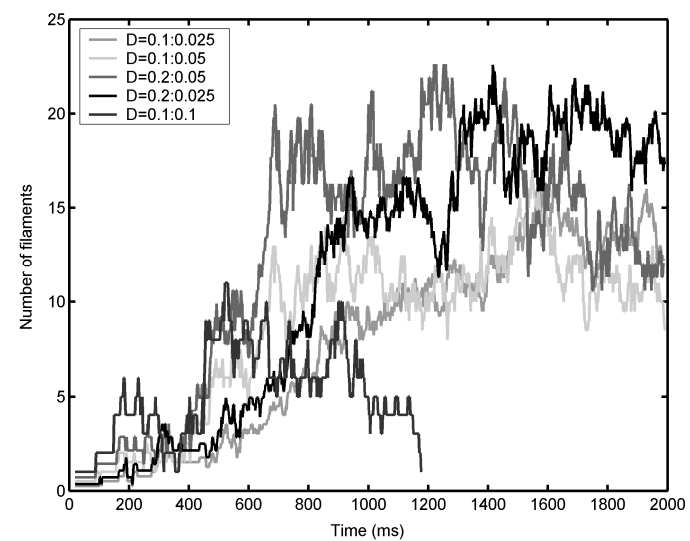
(a)



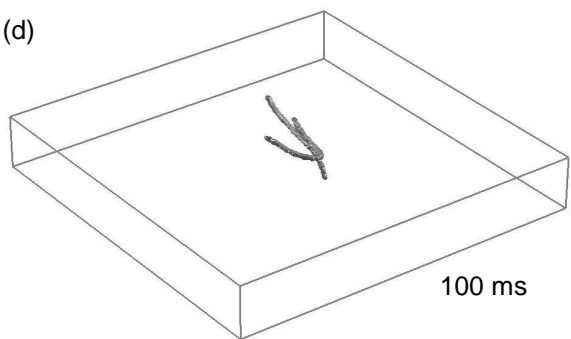
(b)



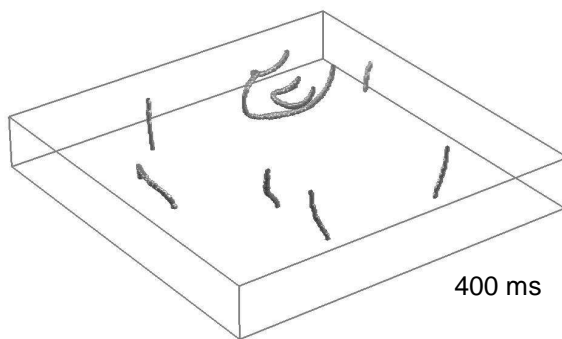
(c)



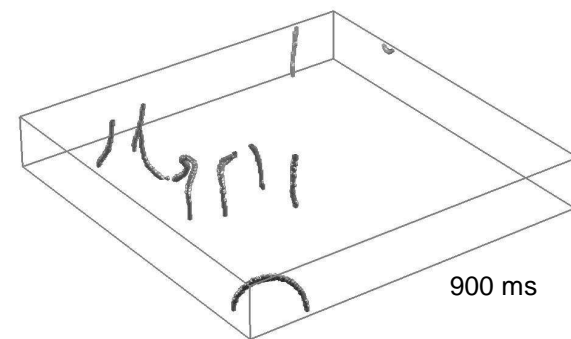
(d)



100 ms

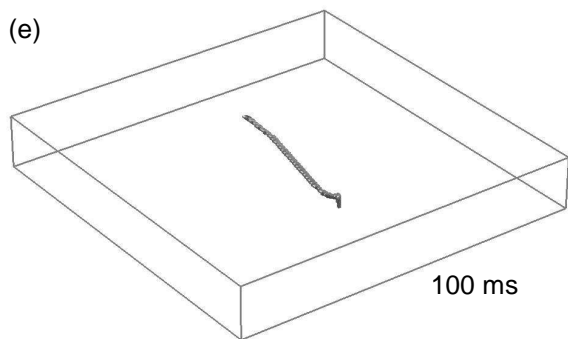


400 ms

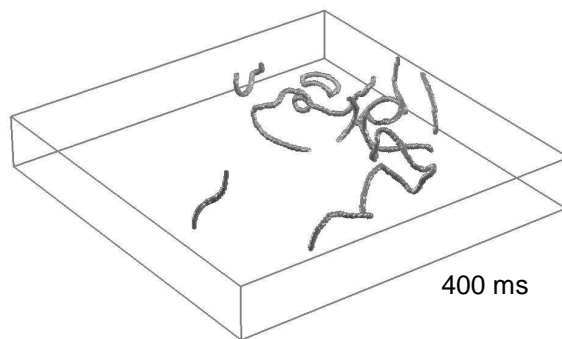


900 ms

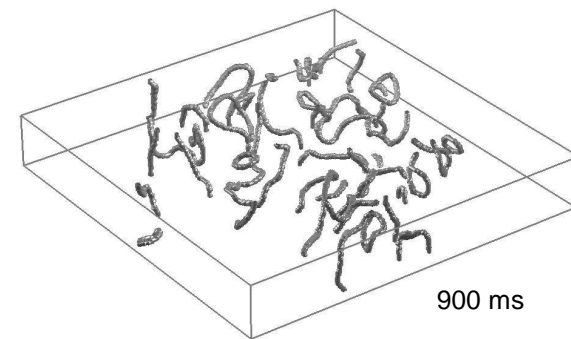
(e)



100 ms



400 ms



900 ms

Figure 5

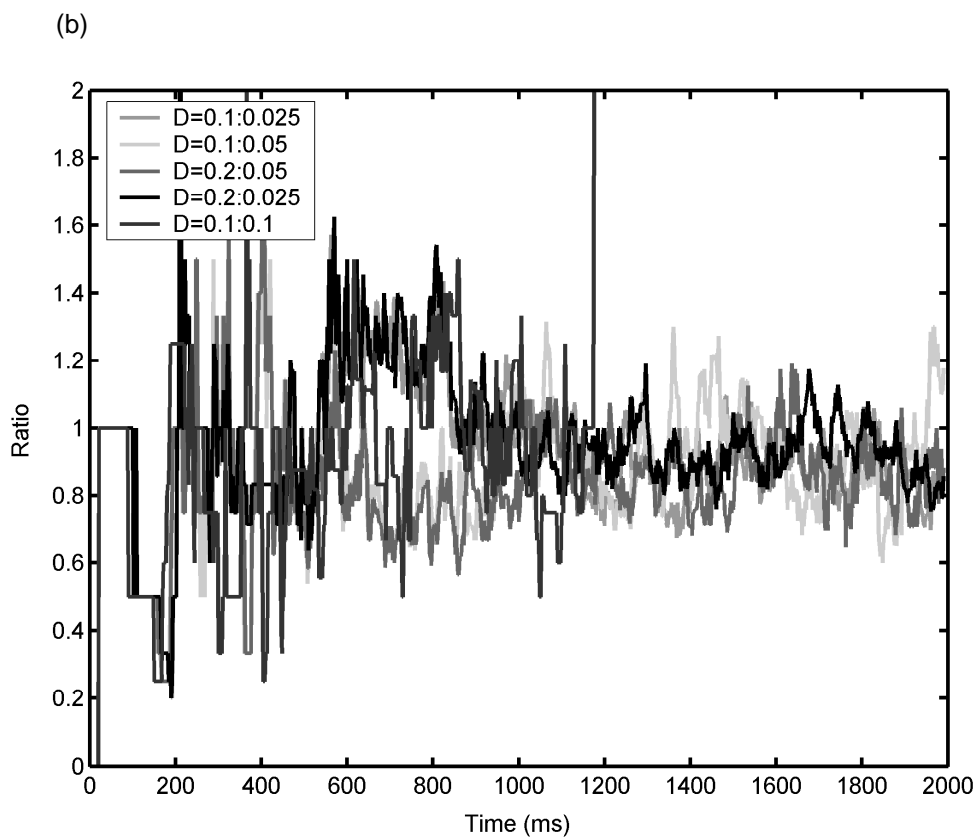
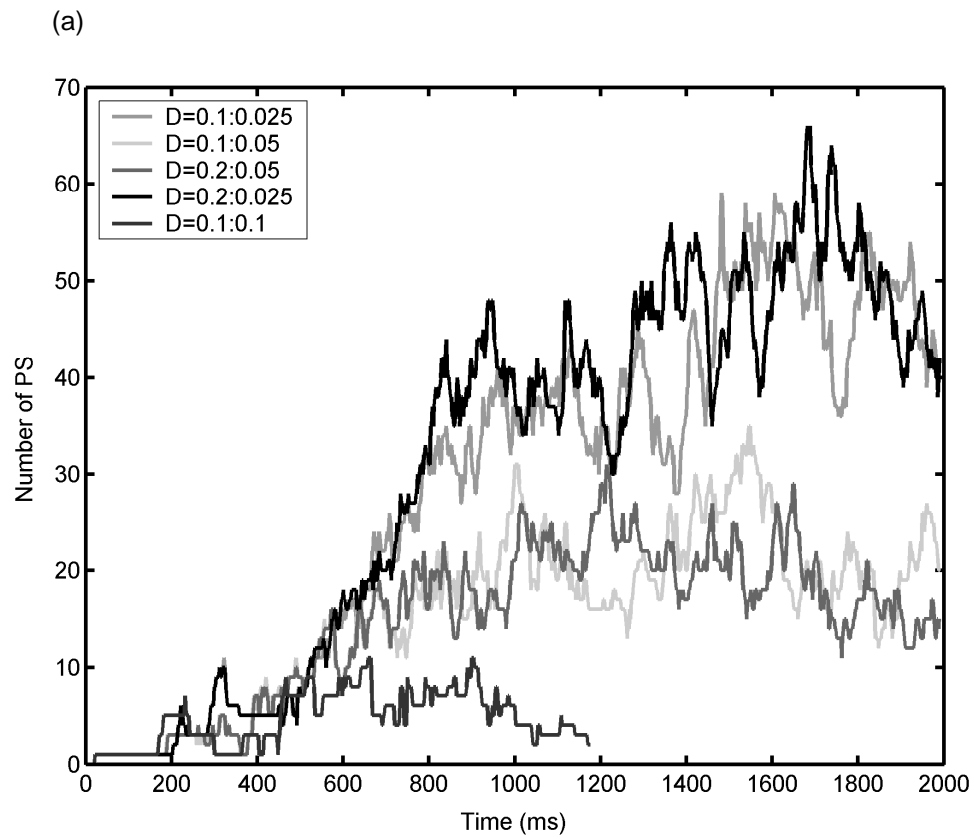


Figure 6

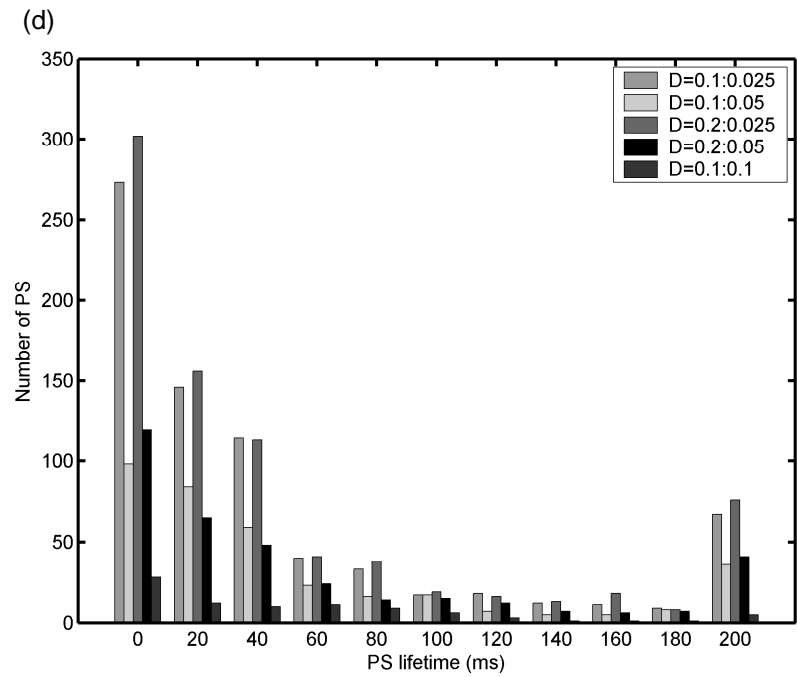
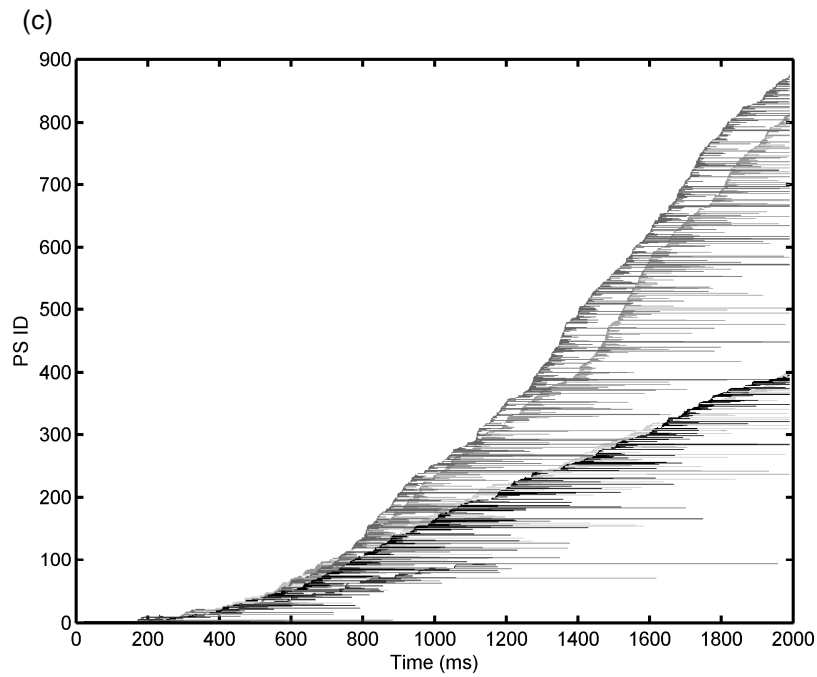
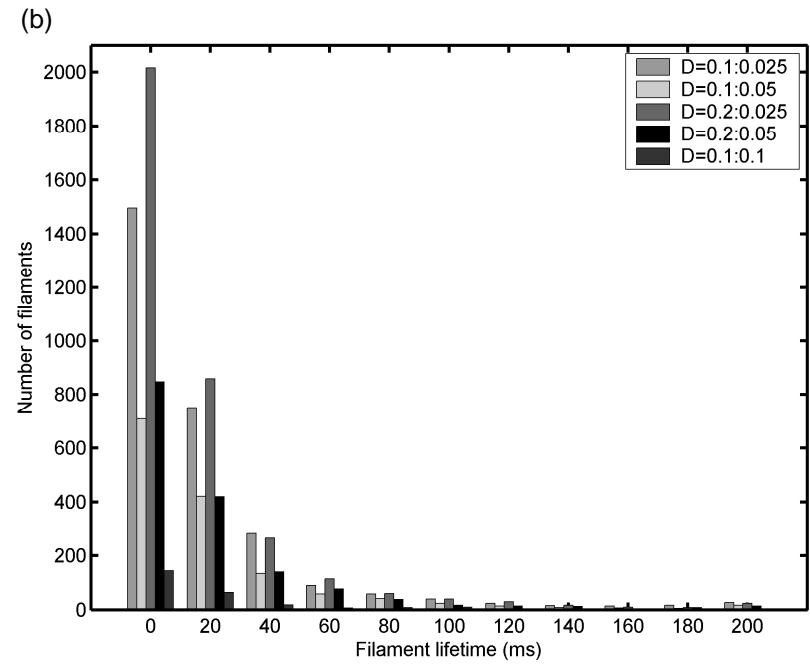
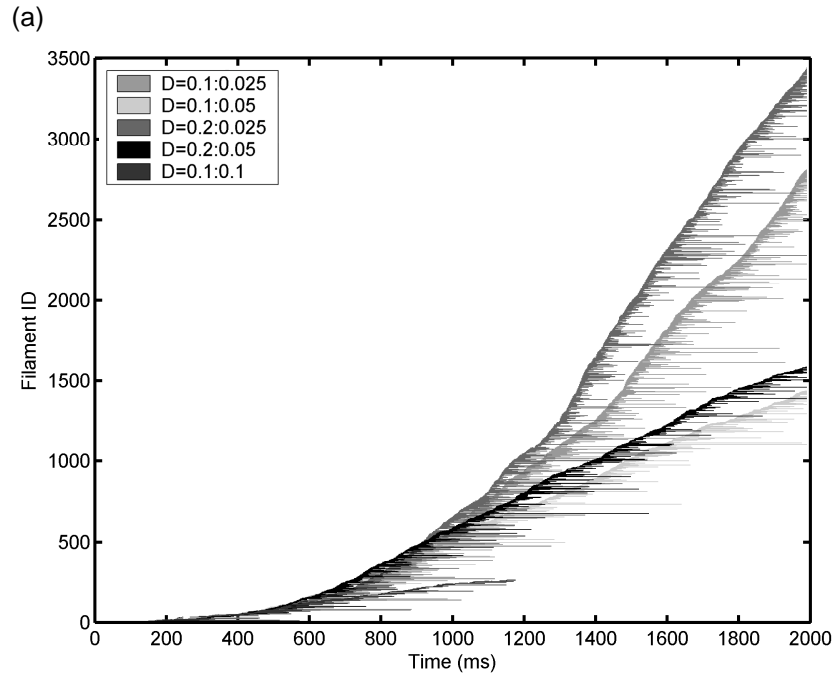
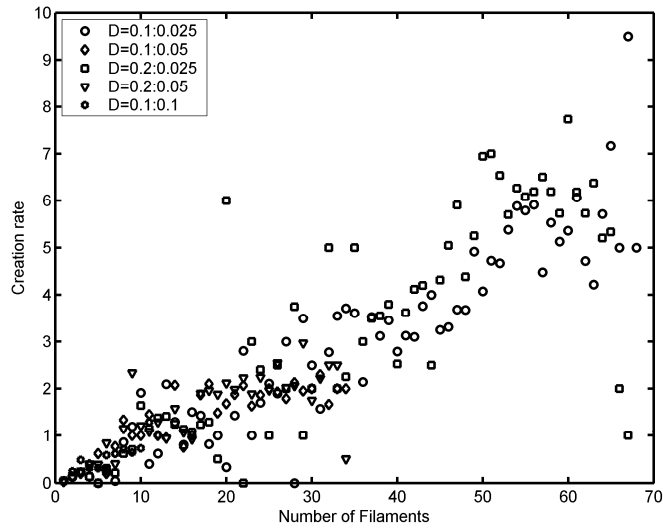
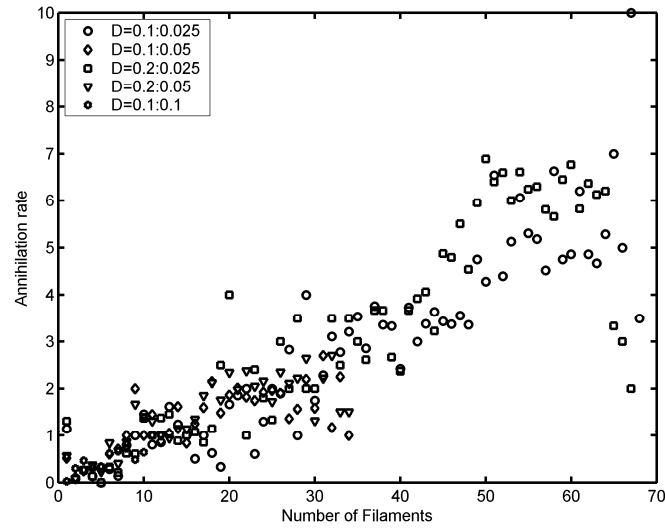


Figure 7

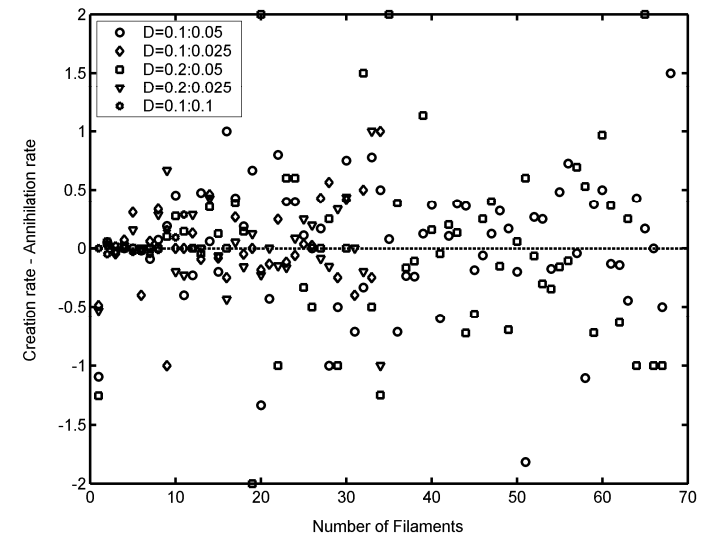
(a)



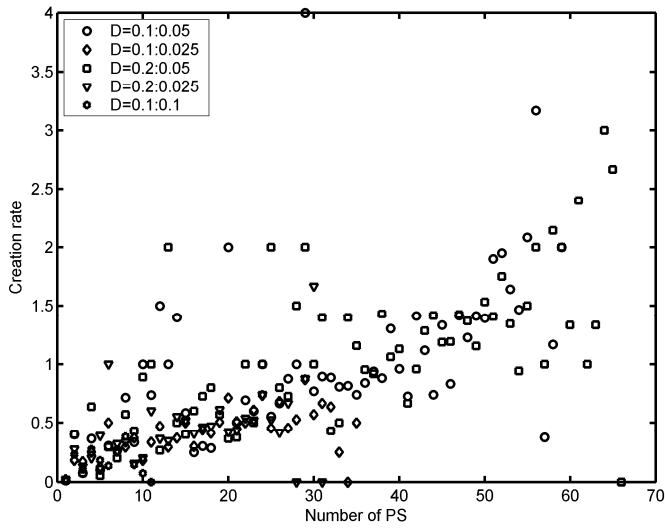
(b)



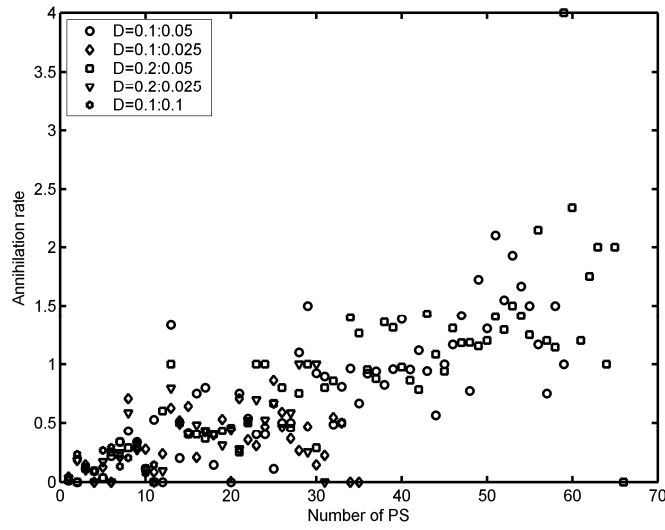
(c)



(d)



(e)



(f)

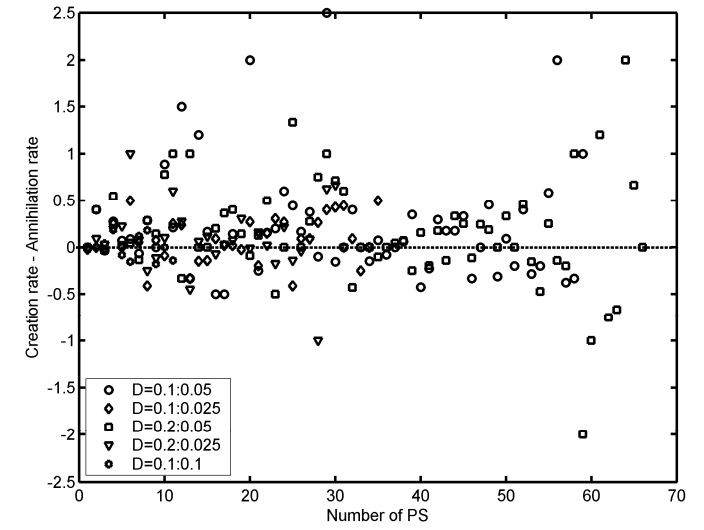


Figure 8

